NANO · MICRO small

Supporting Information

for *Small*, DOI 10.1002/smll.202400570

Decreased Electrically and Increased Ionically Conducting Scaffolds for Long-Life, High-Rate and Deep-Capacity Lithium-Metal Anodes

Chuanfa Li, Jiaqi Wang, Qian Ye, Pengzhou Li, Kun Zhang, Jiaxin Li, Yanan Zhang, Lei Ye, Tianbing Song, Yue Gao, Bingjie Wang and Huisheng Peng**

Supporting Information

Decreased Electrically and Increased Ionically Conducting Scaffolds for Long-Life, High-Rate and Deep-Capacity Lithium-Metal Anodes

Chuanfa Li, Jiaqi Wang, Qian Ye, Pengzhou Li, Kun Zhang, Jiaxin Li, Yanan Zhang, Lei Ye, Tianbing Song, Yue Gao, Bingjie Wang, and Huisheng Peng**

Experimental section

Synthesis of CNT-g-PLiSTFSI bottlebrushes: LiSTFSI monomer and CNT with carbon-carbon double bond grafting sites (CNT-C=C-) were synthesized as described previously.[1] Subsequently, CNT-C=C- (0.2 g) and LiSTFSI (2 g) were added into a 50 mL Schlenk flask containing 20 mL *N,N*-dimethylformamide. The mixture was sonicated for 30 min to obtain a homogeneous suspension. 0.02 g 2,2'-Azobis(2-methylpropionitrile) was then added to the flask, followed by three freeze-pump-thaw cycles. Afterwards, the flask was immersed in an oil bath at 65 °C for 24 h. After the reaction was completed, the product was centrifuged, washed with *N,N*-dimethylformamide for three times and dried in a vacuum.

Characterizations: The morphology and microstructure of the scaffolds were observed by field emission scanning electron microscopy (FESEM, Ultra55). The electrical conductivity microanalysis of the CNT and DEIIC scaffolds was measured through conductive atomic force microscopy (C-AFM, Oxford Cypher VRS1250). The wettability of electrolyte was assessed with a contact angle measurement device (Data

Physics OCA40) and 5 μL electrolyte was dripped onto the scaffolds surface. Fourier transform infrared (FTIR) spectra of CNT and CNT-*g*-PLiSTFSI bottlebrush were performed by IR spectroscopy (Thermofisher Nicolet 6700) with the KBr disk method. X-ray photoelectron spectroscopy (XPS) measurements were carried out with a Thermo Scientific K-Alpha instrument to analyze the elemental composition of the CNT and CNT-*g*-PLiSTFSI bottlebrush. Raman spectroscopies were performed on a HORIBA Scientific LabRAM HR Evolution Raman spectrometer. Thermogravimetric analysis (TGA) was conducted using a Mettler Toledo TGA1 thermogravimetric analyzer under an oxygen atmosphere, with a heating rate of 10 ^{o}C·min^{-1}, ranging from 30 to 800 ^{o}C.

Linear sweep voltammetry test: The LSV test for the electrical conductivity of the CNT and DEIIC scaffolds was performed on the cell configurations in which the CNT and DEIIC electrodes were sandwiched by two stainless steels in the voltage range of 0 to 0.2 V at a scan rate of 1 mV·s^{-1}.

Polarization-interrupt experiment: The CNT-*g*-PLiSTFSI bottlebrushes and poly(vinylidene fluoride) were mixed in a weight ratio of 8:2 with N-methyl-2-pyrrolidone as the solvent. The mixture was then cast onto a Celgard 2325 separator to create the CNT-*g*-PLiSTFSI composite membrane. A similar procedure was followed to prepare the composite CNT membrane. To assemble the Li|Li symmetric cells, the Celgard|CNT-*g*-PLiSTFSI|Celgard or Celgard|CNT|Celgard membranes were fabricated by stacking a bare Celgard separator on the composite membranes to construct a sandwich configuration, which was further sandwiched by two Li electrodes (Figure S27). These two symmetrical cells were used for galvanostatic pulse polarization experiments. The initial step involved performing 5 cycles at 45 μA·cm^{-2} and 45 μAh·cm^{-2} on the cells, which helped establish a stable SEI on the Li electrodes. Subsequently, a concentration gradient-induced polarization (U_0) was established by applying a constant current of 1 mA·cm^{-2} for 5 min in the cell. Following this, the concentration gradient was relaxed by interrupting the current until the cell potential approached zero. The current direction was then reversed, and the process was repeated.

The relaxation of the concentration gradient was observed by monitoring the decay of the cell potential over time. To determine the diffusion coefficient, the long-term relaxation behavior was investigated. The relaxation of the concentration profile could be observed *via* the relaxation of the cell potential $U(t)$. By the mathematical derivation, the effective diffusion coefficient could be calculated from the linear simulated slope m_{ln} in the zone of long-term relaxation:

$$D_{\text{eff}}(C_0) = \frac{l^2}{\pi^2} m_{\ln} \quad (1)$$

Measurement of the Li^+ transference number: The t_{Li+} was determined using the potentiostatic polarization method at an applied voltage polarization of 0.01 V. The cell configuration used for this measurement was the same as the above polarization-interrupt experiment. The polarization of symmetric cells and their serial Nyquist plots before and after polarization were used to calculate t_{Li+} based on the following equation:

$$t_{Li^+} = \frac{I_s(\Delta V - I_0 R_0)}{I_0(\Delta V - I_s R_s)} \quad (2)$$

Asymmetrical and symmetrical cell tests: The electrochemical performances were measured in 2032 coin cells. CNT-*g*-PLiSTFSI bottlebrushes and poly(vinylidene fluoride) with a weight ratio of 8:2 were mixed in N-methyl-2-pyrrolidone and then casted onto Cu foil to prepare the DEIIC scaffold. Bare Cu foil and CNT were used as the control working electrodes for comparison. Asymmetrical Cu|Li cells were assembled with Celgard 2325 separators, Li foil counter electrodes and 30 μL electrolyte of 1.0 M LiTFSI in a mixture of DOL and DME (1:1 by volume) with 2 wt% $LiNO_3$ additive in an Ar-filled glove box.

CV of the asymmetric cells with CNT and DEIIC scaffolds were measured in the potential range from −0.2 V (*vs.* Li^+/Li) to initial potentials of the cells with a scan rate of 0.2 $mV \cdot s^{-1}$. EIS was performed in the frequency range of 100 kHz to 0.01 Hz with an alternating voltage amplitude of 5 mV. The CV and EIS tests were conducted by an electrochemical station (CHI660E, Chenhua).

The cells were first cycled from 0 to 1 V at ~45 μA·cm^{-2} for 5 cycles to attain stable SEI layers. To calculate the CE of repeated Li plating/stripping for asymmetric cells, Li was repeatedly plated onto the Cu foil at 1 mA·cm^{-2} with a fixed Li deposition amount of 1 mAh·cm^{-2}, followed by stripping at the same areal current density until the voltage reached 1 V *vs.* Li/Li^{+}. For the symmetrical cell test, 5 mAh·cm^{-2} of Li was first pre-plated onto the working electrodes at 1 mA·cm^{-2}, and then the cells were cycled at various current densities with diverse areal capacities. The GITT voltage profiles of the symmetric cells were measured with a periodically interrupted current (1 mA·cm^{-2} for 30 min) and a resting time of 60 min until the overall plating/stripping areal capacity was 4 mAh·cm^{-2}.

Full cell tests: In the full cells, the DEIIC scaffolds or the bare Cu electrodes pre-plated with 6 or 10 mAh·cm^{-2} of Li were used as the anodes and NCM622 electrodes with the mass loading of 21.6 mg·cm^{-2} were used as the cathodes. The electrolyte was a ternary electrolyte containing $LiPF_6$ in ethylene carbonate–diethyl carbonate–ethyl methyl carbonate (KLD-1230C, Guangdong Canrd New Energy Technology). Celgard 2325 was used as the separator. The galvanostatic charge/discharge tests were performed by a LAND battery tester at different current densities within a cutoff voltage window of 3.0–4.3 V.

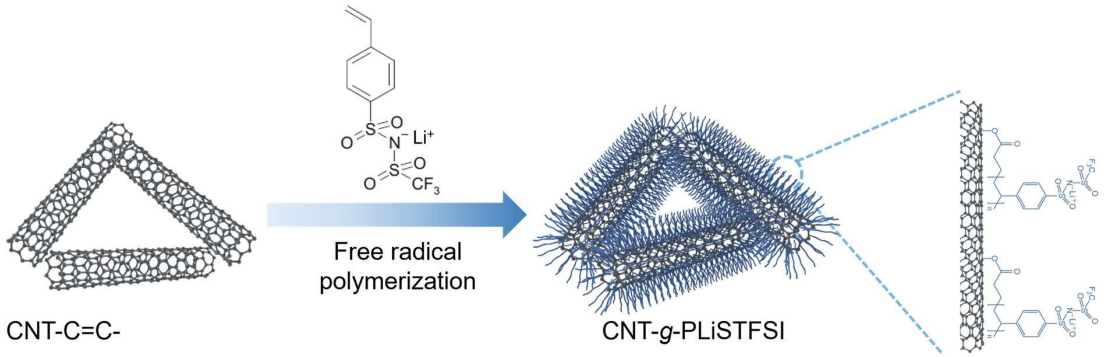

Figure S1. Schematic illustration of the polymer grafting process from the surfaces of CNTs. First of all, hydroxylate CNTs were modified by acryloyl chloride to introduce carbon-carbon double bonds as grafting sites. Subsequently, the hairy PLiSTFSI chains were grafted from the modified sites of CNTs *via* surface-initiated free radical polymerization, leading to the synthesis of hybrid bottlebrushes, *i.e.*, PLiSTFSI-grafted carbon nanotube (CNT-*g*-PLiSTFSI).

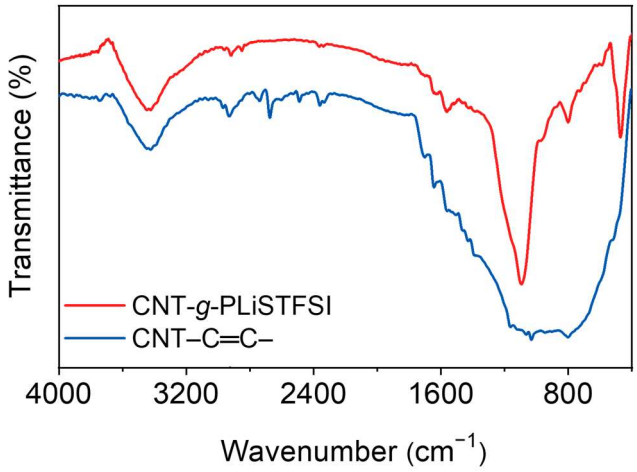

Figure S2. FTIR spectra of CNT and CNT-*g*-PLiSTFSI. The FTIR spectra revealed that the PLiSTFSI chains were successfully grafted from the CNT, as demonstrated by the presence of two new characteristic peaks of methylene groups at 2920 and 2850 cm^{-1};[2] and the two strong characteristic peaks at 1203 and 1095 cm^{-1} for CNT-*g*-PLiSTFSI were ascribed to the asymmetric and symmetric stretch of sulfonyl groups.[3]

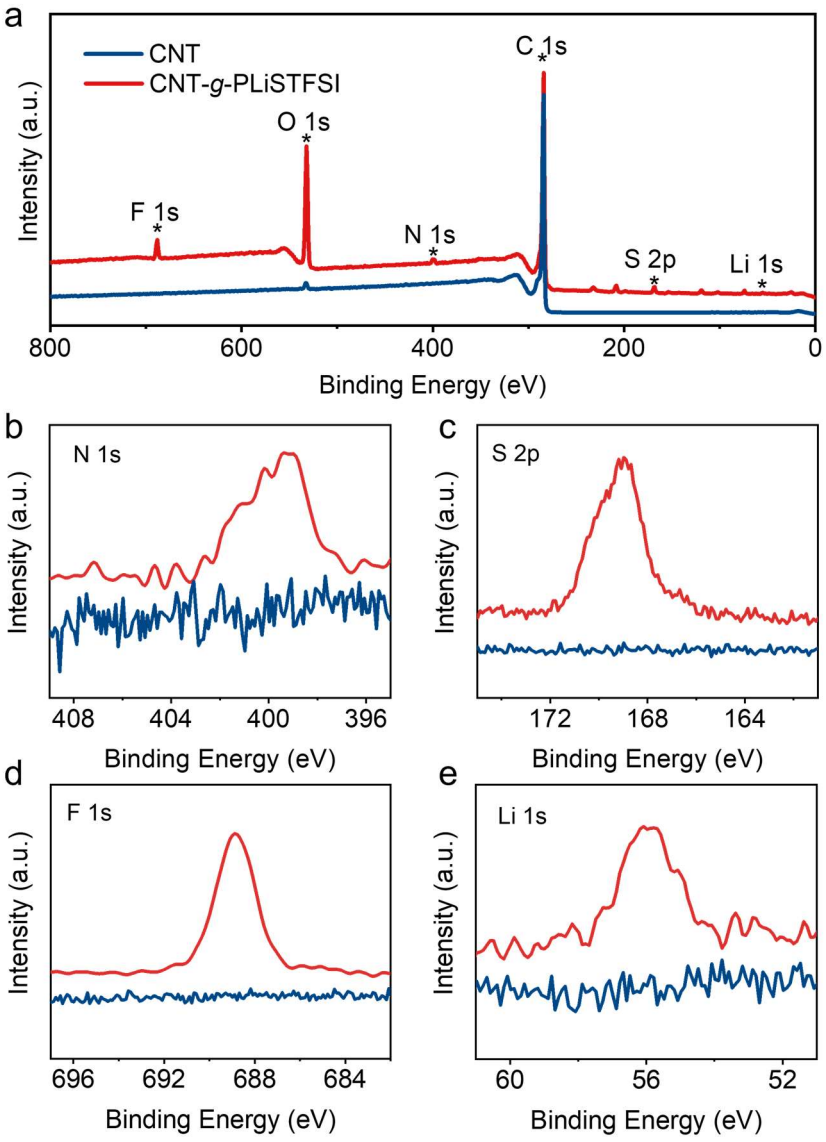

Figure S3. (**a**) XPS spectra and corresponding high-resolution (**b**) N 1s, (**c**) S 2p, (**d**) F 1s and (**e**) Li 1s XPS spectra of CNT and CNT-*g*-PLiSTFSI. XPS analysis of CNT-*g*-PLiSTFSI confirmed the presence of N, S, F, and Li peaks, providing additional evidence for the successful surface grafting of PLiSTFSI on CNT.

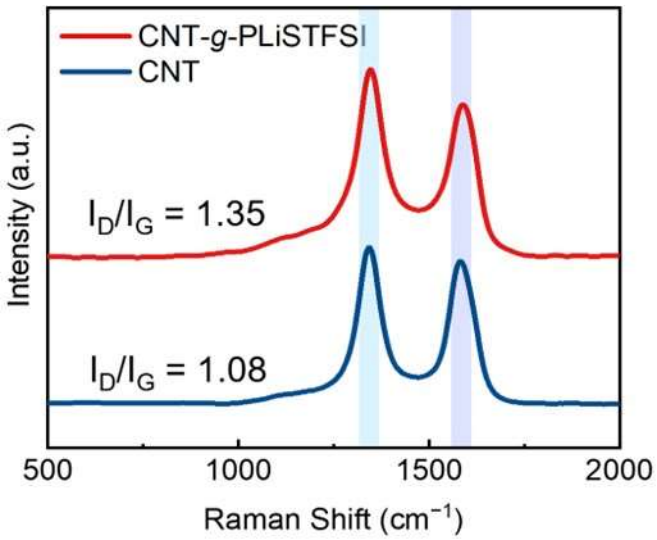

Figure S4. Raman spectra of CNT and CNT-*g*-PLiSTFSI. The Raman spectra showed an increased intensity ratio of the disorder-induced D band to the first-order graphite G band (I_D/I_G) after the grafting process, indicating an increased disorder degree of CNTs due to the grafting of PLiSTFSI chains.[4]

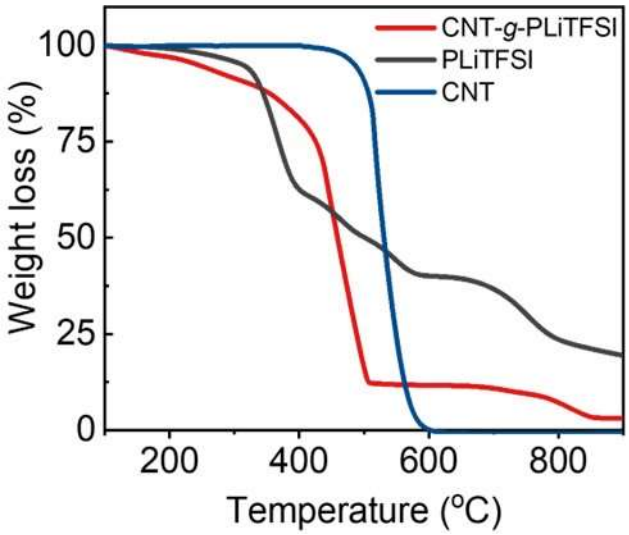

Figure S5. TGA curves of CNT, PLiSTFSI and CNT-*g*-PLiSTFSI obtained under O_2 atmosphere.

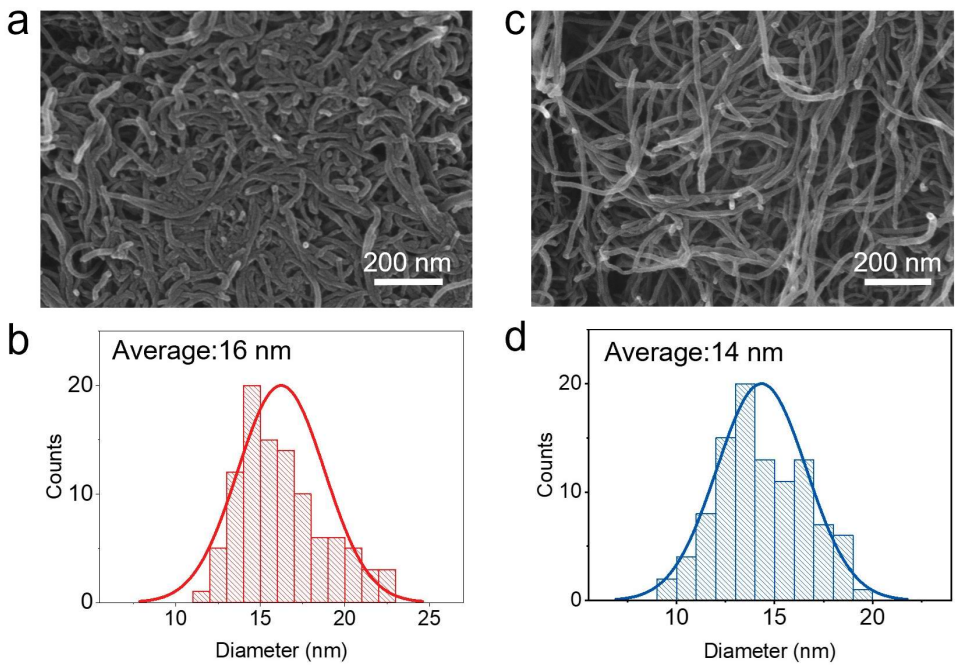

Figure S6. (**a**, **c**) SEM images and corresponding (**b**, **d**) diameter distribution histograms of (**a**, **b**) CNT-*g*-PLiSTFSI and (**c**, **d**) CNT.

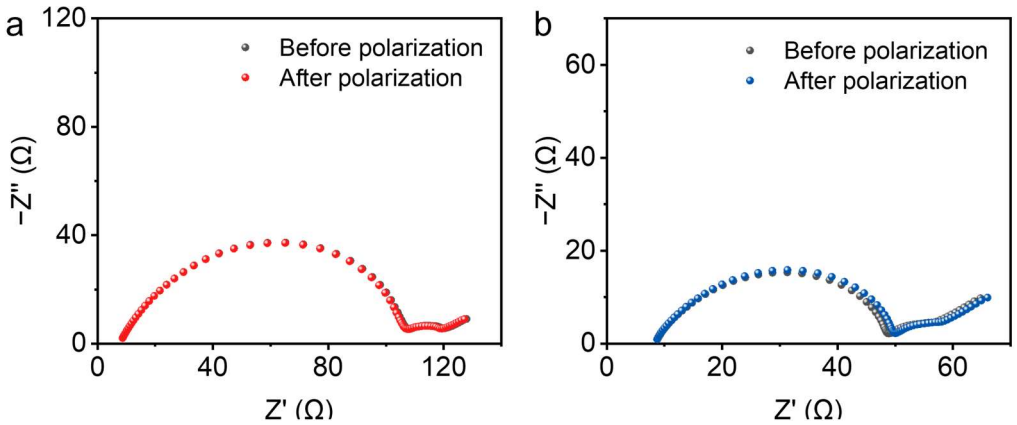

Figure S7. Nyquist impedance plots of symmetric cells with (**a**) CNT-*g*-PLiSTFSI and (**b**) CNT membranes before and after polarization.

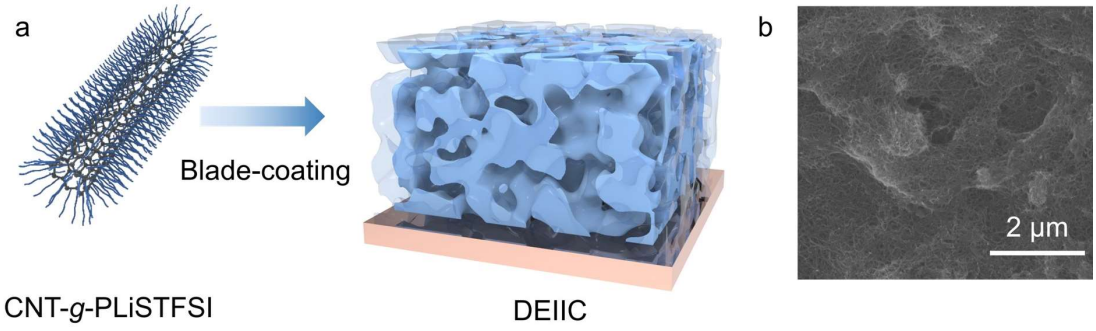

Figure S8. (**a**) Schematic showing the fabrication of the DEIIC scaffold. (**b**) SEM image of the DEIIC scaffold by top view.

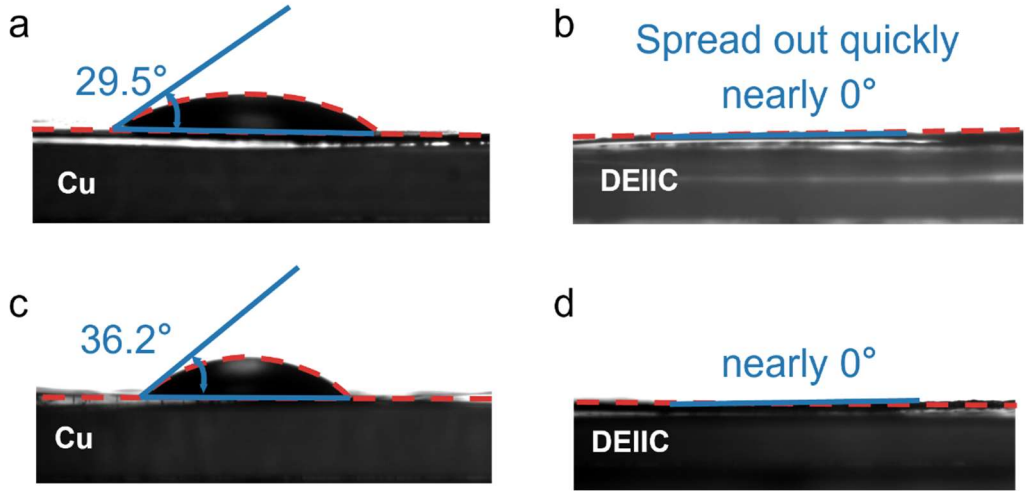

Figure S9. Contact angles of (**a**, **b**) ether- and (**c**, **d**) carbonate-based electrolytes on the (**a**, **c**) Cu and (**b**, **d**) DEIIC scaffolds.

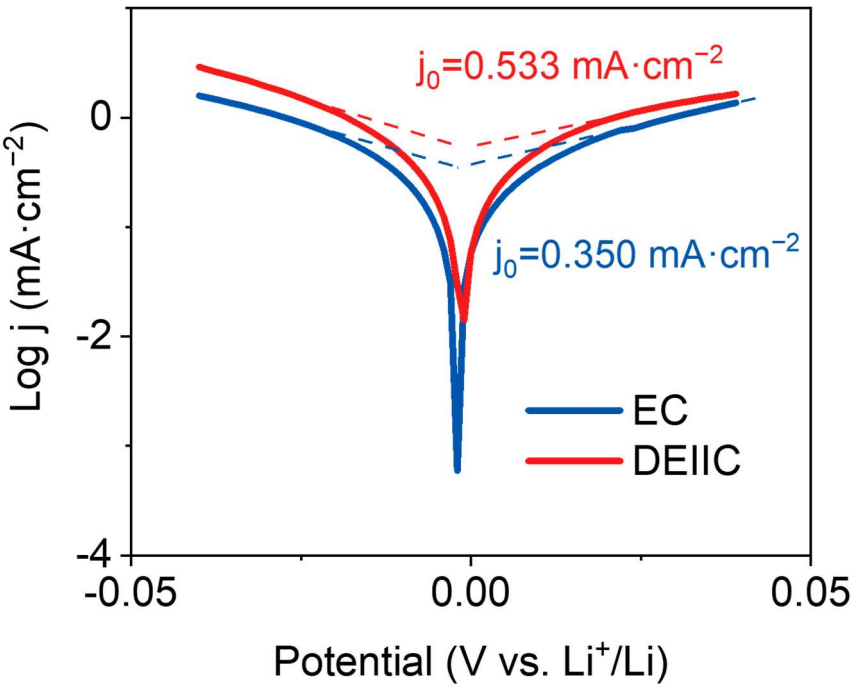

Figure S10. Tafel plots calculated from the CV curves of asymmetric cells with DEIIC and EC scaffolds.

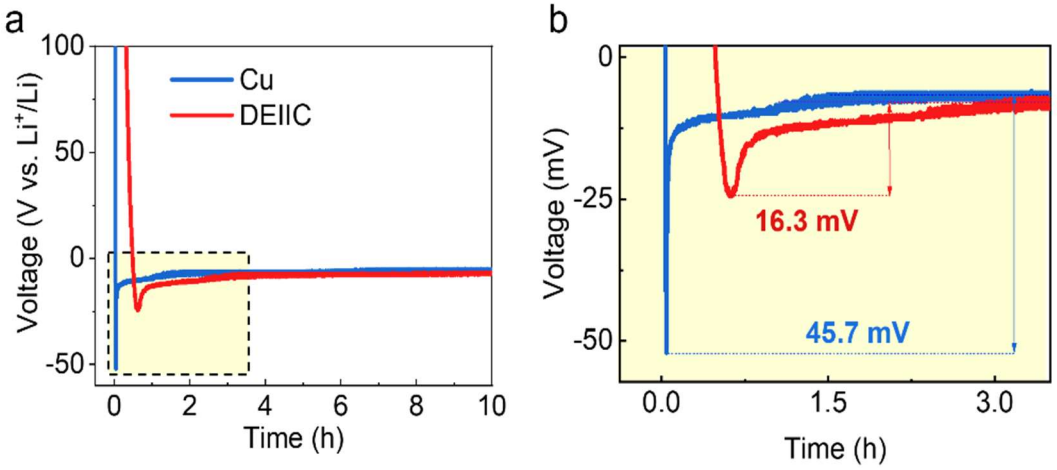

Figure S11. (**a**) Voltage profiles of Li plating on bare Cu foils and DEIIC scaffolds at 45 μA·cm^{-2} and (**b**) corresponding local magnified profiles.

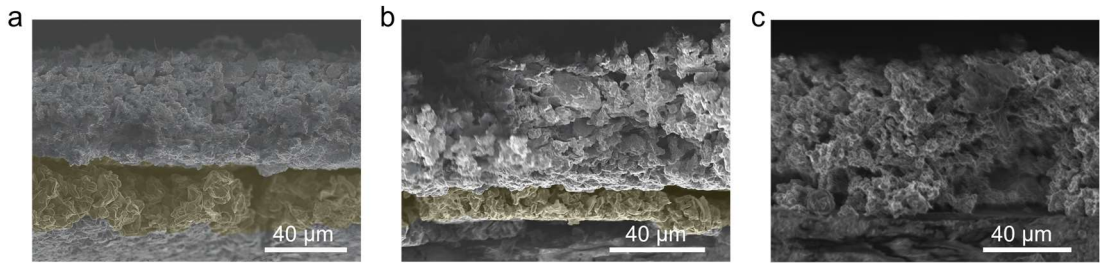

Figure S12. Cross-sectional SEM images of the DEIIC scaffolds pre-deposited with 5 mAh·cm^{-2} of Li and subsequently stripped (**a**) 1, (**b**) 3, and (**c**) 5 mAh·cm^{-2} of Li at 1 mA·cm^{-2}.

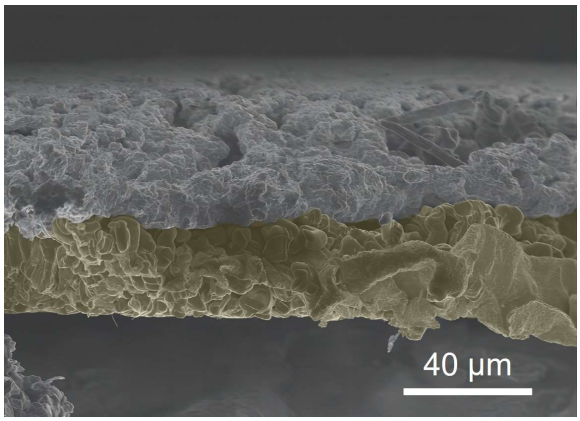

Figure S13. Cross-sectional SEM image of the DEIIC scaffold pre-deposited with 5 mAh·cm^{-2} of Li after a cycle at 1 mA·cm^{-2} and 3 mAh·cm^{-2}.

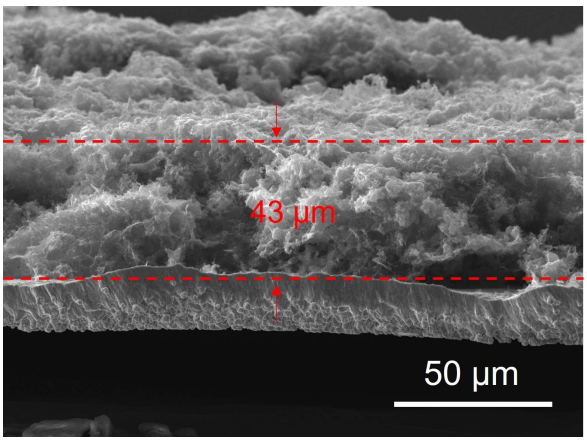

Figure S14. Cross-sectional SEM image of the thinner DEIIC scaffold.

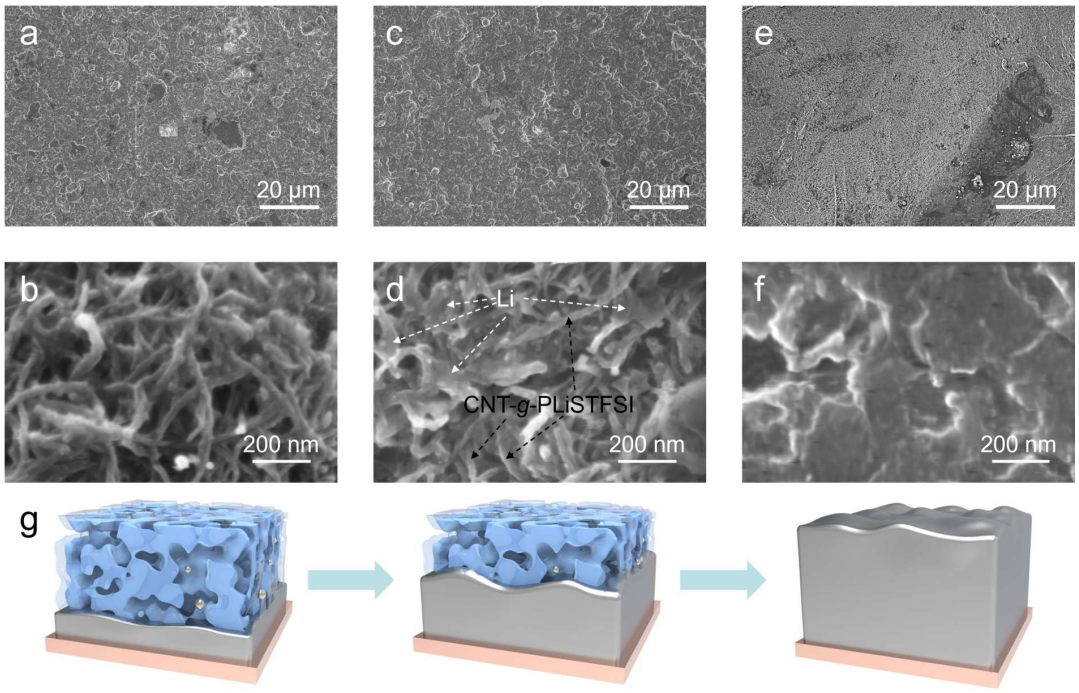

Figure S15. SEM images of Li deposited on the DEIIC scaffolds with capacities of (**a**, **b**) 1 mAh·cm^{-2}, (**c**, **d**) 3 mAh·cm^{-2} and (**e**, **f**) 6 mAh·cm^{-2} by top view. (**g**) Schematic diagram showing bottom–up plating behavior of Li within the DEIIC scaffold.

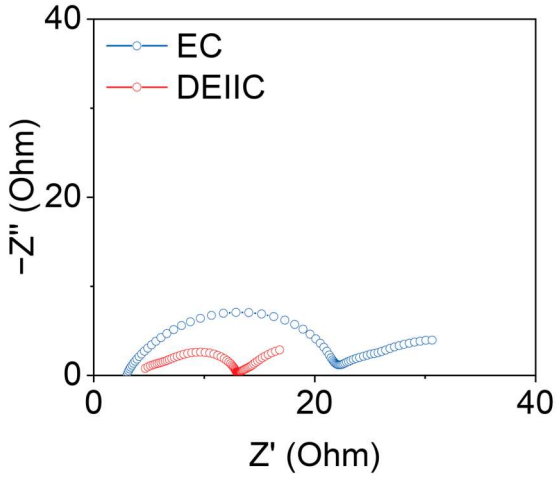

Figure S16. Nyquist impedance plots of asymmetric cells with DEIIC and EC scaffolds after plating 5 mAh·cm^{-2} of Li within the scaffolds.

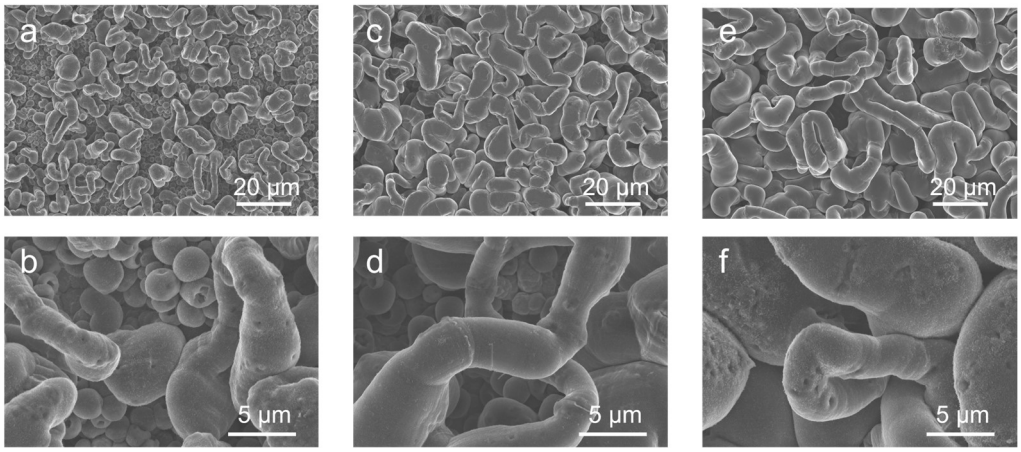

Figure S17. SEM images of Li deposited on the bare Cu electrode with a capacity of (**a**, **b**) 1, (**c**, **d**) 3 and (**e**, **f**) 6 mAh·cm^{-2} by top view.

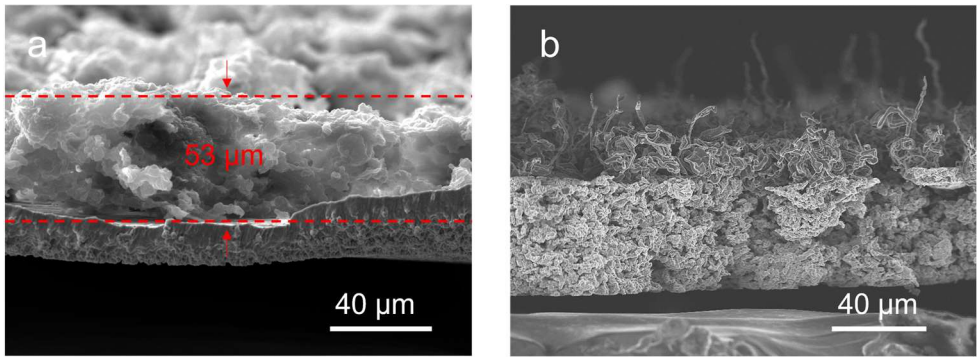

Figure S18. Cross-sectional SEM images of the EC scaffolds (**a**) before and (**b**) after plating 1 mAh·cm^{-2} of Li at 1 mA·cm^{-2}.

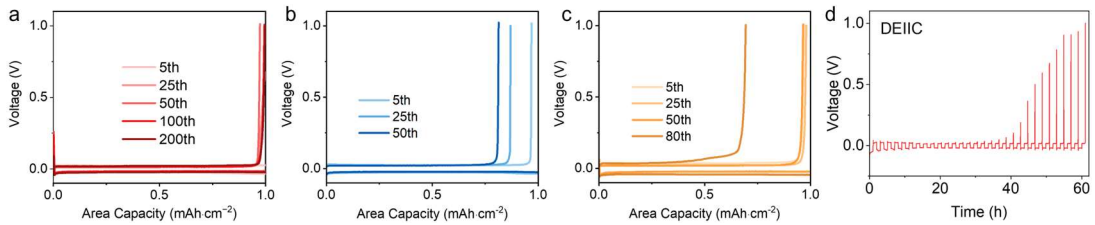

Figure S19. Voltage profiles of Li plating/stripping processes in the asymmetrical cells with (**a**) DEIIC, (**b**) Cu and (**c**) EC scaffolds. (**d**) Time-voltage curve of the asymmetrical cell with DEIIC scaffold at 1 mA·cm^{-2} and 1 mAh·cm^{-2} for the first 30 cycles.

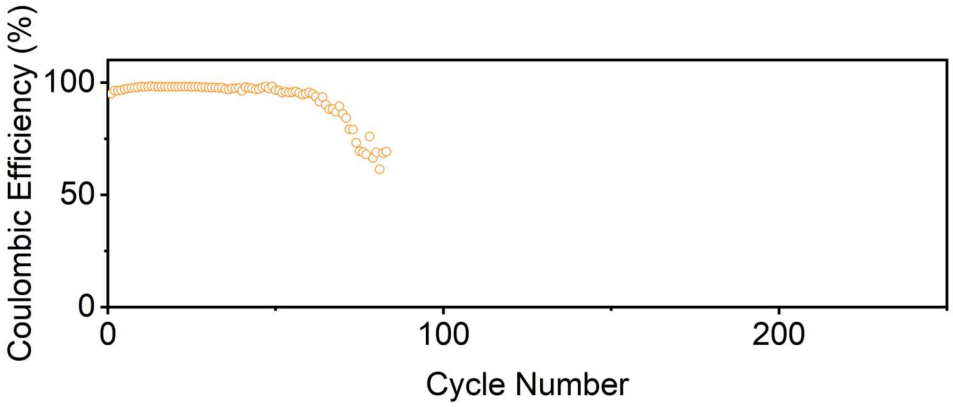

Figure S20. CE of asymmetrical cell with EC scaffold with a cycling capacity of 1 mAh·cm^{-2} at a current density of 1 mA·cm^{-2}.

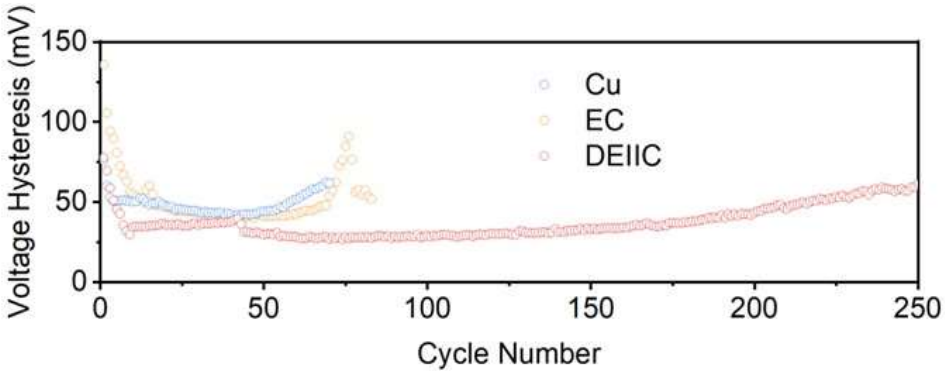

Figure S21. Voltage hysteresis of Li metal plating/striping in the asymmetrical cells with the bare Cu, EC and DEIIC scaffold.

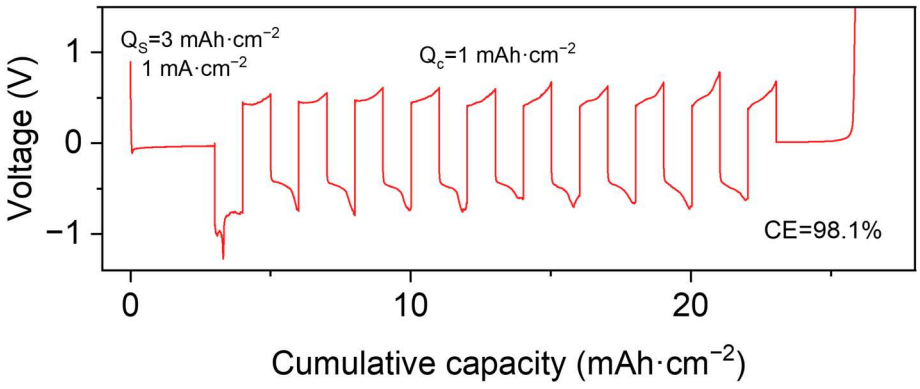

Figure S22. Voltage profile of DEIIC scaffold for CE test using the "reservoir" method at 50 mA·cm^{-2}.

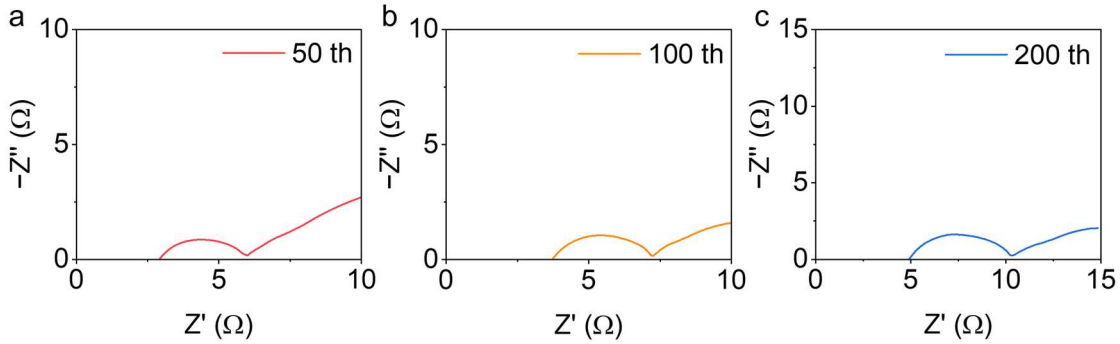

Figure S23. Nyquist impedance plots of symmetric cells with DEIIC scaffolds after (**a**) 50, (**b**) 100 and (**c**) 200 cycles.

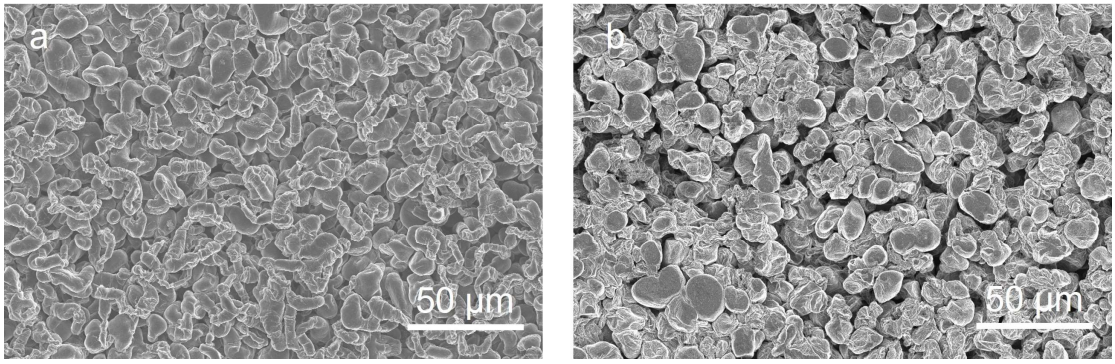

Figure S24. SEM images Li@Cu electrode in the symmetric cell after (**a**) 10 and (**b**) 100 cycles with an areal capacity of 1 mAh·cm^{-2} at 1 mA·cm^{-2} by top view.

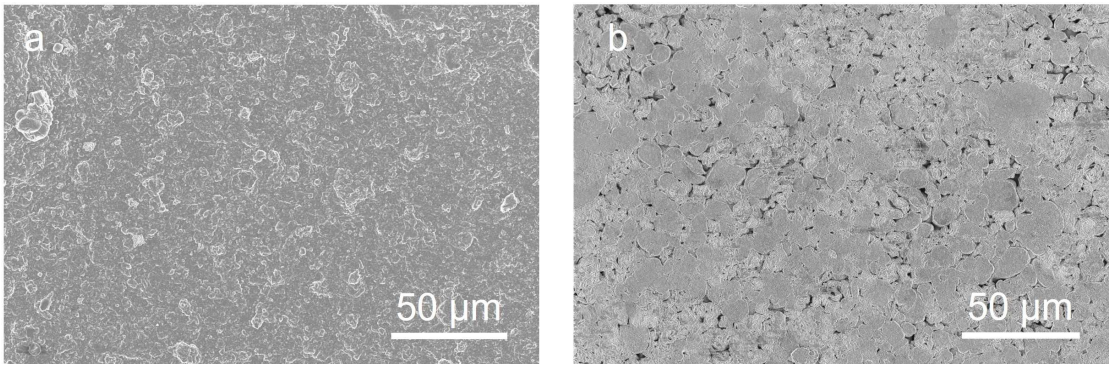

Figure S25. SEM images Li@DEIIC electrode in the symmetric cell after (**a**) 10 and (**b**) 100 cycles with an areal capacity of 1 mAh·cm^{-2} at 1 mA·cm^{-2} by top view.

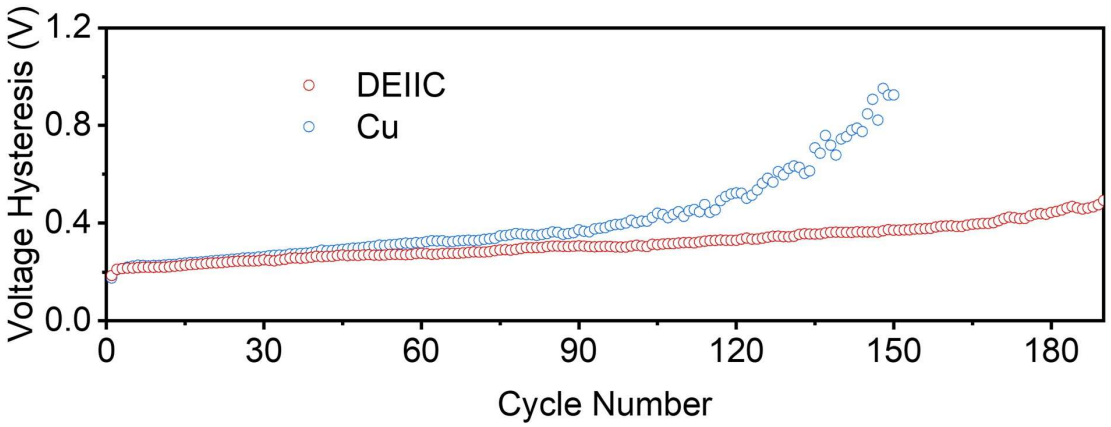

Figure S26. Voltage hysteresis of full cells with bare Cu and DEIIC scaffold.

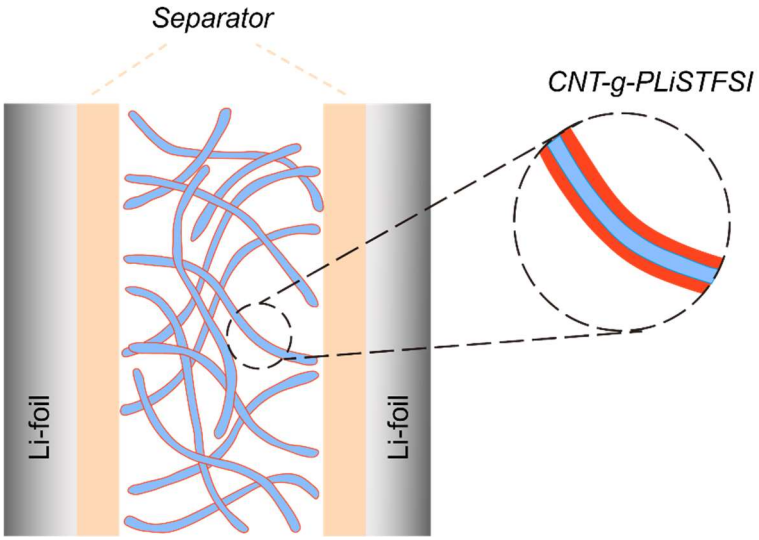

Figure S27. Schematic illustration of a symmetric cell configuration for testing diffusion coefficients.

Table S1. Porosities of the EC and DEIIC scaffolds.

Parameter	EC scaffold	DEIIC scaffold
The areal density of the dry electrode	11.74 mg·cm^{-2}	12.00 mg·cm^{-2}
The areal density of the electrode after absorbing the electrolyte	15.96 mg·cm^{-2}	17.12 mg·cm^{-2}
The thickness of scaffolds	53 μm	66 μm
Electrolyte density	0.96 g·mL^{-1}	0.96 g·mL^{-1}
Porosity	83%	80%

Table S2. Calculation of the energy density of the full cell with limited excess Li and lean electrolyte.

Component	Data
Plating lithium metal (6 mAh cm^{-2})	1.6 mg·cm^{-2}
DEIIC scaffold	0.7 mg·cm^{-2}
NCM622 cathode	21.6 mg·cm^{-2}
Celgard2325 separator	1.6 mg·cm^{-2}
Electrolyte	E/C=4.2 g·Ah^{-1}
Discharge capacity	3.2 mAh·cm^{-2}
Average discharge voltage	3.7 V
Total stack energy	11.8 mWh·cm^{-2}
Total stack weight	38.9 mg·cm^{-2}
Stack gravimetric energy density	303.3 Wh·kg^{-1}

References for the Supporting Information

[1] Y. Lin, Y. Zhu, Q. Ma, X. Ke, P. Ma, R. Liao, S. Liu, D. Wu, *Macromol. Rapid Commun.* **2022**, 43, 2100915.

[2] C. Li, S. Liu, C. Shi, G. Liang, Z. Lu, R. Fu, D. Wu, *Nat. Commun.* **2019**, 10, 1363.

[3] M. Zhou, R. Liu, D. Jia, Y. Cui, Q. Liu, S. Liu, D. Wu, *Adv. Mater.* **2021**, 33, 2100943.

[4] a) L. G. Bulusheva, A. V. Okotrub, I. A. Kinloch, I. P. Asanov, A. G. Kurenya, A. G. Kudashov, X. Chen, H. Song, *Phys. Status Solidi B* **2008**, 245, 1971; b) J. Huang, Y. Lin, S. Liu, Q. Liu, Y. Sun, Y. Liang, Y. Chen, R. Fu, D. Wu, *Chem. Commun.* **2018**, 54, 10332.